Effects of Supercritical Carbon Dioxide on Phase Homogeneity, Morphology, and Mechanical Properties of Poly(styrene-*blend*-ethylene-*stat*-vinyl acetate)

E. Palermo,*,† M. Si,⊥ R. Occhiogrosso,‡ C. Berndt,§ Gregory Rudomen,# and M. Rafailovich*,⊥

Sibley School of Mechanical & Aerospace Engineering, Cornell University, 303 Bard Hall, Ithaca, New York 14853; Hebrew Academy of the Five Towns and Rockaway (HAFTR) High School, Cedarhurst, New York 11516; School of Engineering, James Cook University, Townsville, QLD 4811, Australia; Department of Materials Science & Engineering, State University of New York at Stony Brook, Stony Brook, New York 11794-2275; and University Hospital and Medical Center, State University of New York at Stony Brook, Stony Brook, New York 11794-8008

Received June 23, 2005; Revised Manuscript Received August 28, 2005

ABSTRACT: Significant enhancement of the mechanical properties in PS/EVA blends is achieved via sc CO_2 exposure in the pressure/temperature domain where the amplitude of the density fluctuations is maximal. Before exposure, bulk samples of the blends elongate an average of 134% under uniaxial tension, whereas the average elongation is 682% after exposure. SEM micrographs of the exposed blends indicate that foams with pores roughly 5−15 μm in diameter, separated by splines 1−2 μm wide, are formed at all pressures higher than 800 psi. We attribute the enhancement of the mechanical properties in PS/EVA to an increased degree of miscibilization of the immiscible polymers along the spline surfaces. When foaming occurs, the surface-to-volume ratio is increased, thereby increasing the regions where surface miscibilization can occur. Since tensile stresses in the material are sustained by the splines, reinforcement of the mechanical properties in this specific area results in an overall enhancement of the tensile properties of the material. The increased miscibility was further confirmed by contact angle and DSC measurements of the blends before and after exposure. The results showed a decrease in the contact angle from 18° to 3° and the appearance of a second glass transition, which was intermediate between the T_g values of the PS and EVA homopolymers.

1. Introduction

Supercritical carbon dioxide (sc CO_2) has long been used in polymer processing because it is environmentally safer than other solvents, such as chlorofluorocarbons, and has a convenient critical point of T_c = 31.3 °C (near ambient) and P_c = 1073 psig.[1] For these reasons, sorption and swelling of a wide variety of bulk polymers in CO_2 have been studied by numerous authors.[3,4,6] Their work has frequently focused on the foaming process, since the miscibility in sc CO_2 with most polymers is low, and they have shown that sc CO_2 can be an effective foaming agent where the pore dimensions can be controlled by M_w, polydispersity,[2] and foaming temperature.[3] Regarding polymer blends, Elkovitch et al. found a decrease in phase dispersion[7] and viscosity[8] when sc CO_2 was injected during melt extrusion of two-component polymer blends. Similarly, Walker, et al. report enhanced miscibility in certain blends after exposure to sc CO_2.[9] Still, in contrast to the large body of literature on homopolymers,[10−20] relatively little has been reported regarding the surface miscibilization and concurrent foaming effects of sc CO_2 in bulk polymer blends. Since immiscible polymers will phase segregate into micron-sized domains far larger than the regions between pores (referred to as "splines") when melt extruded, questions as to the effect of the phase separation on the foaming process arise.

Recently, Nishikawa et al.[21−23] have shown that in a certain pressure−temperature locus sc CO_2 exhibits drastic density fluctuations. Koga et al.[24,25] have shown that in this regime, also known as the "ridge", sc CO_2 becomes a powerful solvent for a large number of polymers, where it would be otherwise immiscible. Furthermore, they showed that significant interfacial broadening between immiscible polymer thin films occurs when exposed to sc CO_2 along the ridge.[26] This effect had not been previously observed in bulk studies since it is strongest near the surface where the amplitude of the density fluctuations is large. Since the diameter of the splines in a foamed material is on the order of the penetration depth of the sc CO_2 in the density fluctuation regime, it is interesting to observe whether the surface solvent effect reported by Koga et al.[24,25] can act as a potential miscibilizing agent of the foamed bulk blend.

We investigated a model blend of poly(styrene-*blend*-ethylene-*stat*-vinyl acetate), which we refer to as "PS/EVA". These polymers were chosen since they are individually well characterized, and the bulk properties have been studied extensively in sc CO_2.[5,27] Furthermore, since their mechanical properties are complementary, when combined in the appropriate ratio, they can potentially produce a high-modulus, impact-resistant material.

We first determine the effect of sc CO_2 on the miscibility of PS/EVA spun-cast thin films in the pressure−temperature regime where the effect reported by

† Cornell University.
‡ HAFTR High School.
§ James Cook University.
⊥ Department of Materials Science & Engineering, SUNY.
University Hospital and Medical Center, SUNY.
* Corresponding authors: E-mail efp9@cornell.edu or mrafailovich@notes.cc.sunysb.edu.

10.1021/ma051335+ CCC: $30.25
Published on Web 10/06/2005

Table 1. Polymer Physiochemical Characteristics

material	M_w (g/mol)	M_w/M_n	T_m (°C)	T_g (°C)	surface tension γ (dyn/cm)
polystyrene	45K	>2.0		100	36
ethylene vinyl acetate (ELVAX 360, 25% VA)	100K	>2.0	78	−30	31

Koga et al.[24,25] is expected to be maximal. We then study the effect on bulk samples mechanically blended in a C. W. Brabender twin-screw melt mixer. The dynamic properties of the blends were measured using dynamic mechanical analysis (DMA) and tensile testing, as they vary with the sc CO_2 temperature and pressure of exposure. The results are correlated to SEM images of the internal morphology of bulk samples as well as determination of the interfacial tensions between the polymers, as determined from contact angle measurements in thin films.

2. Experimental Section

2.1. Polymer Selection. In this study, ca. 45K M_w polystyrene from Sigma-Aldrich and ca. 100K M_w poly(ethylene-*stat*-vinyl acetate) with 25 wt % vinyl acetate (ELVAX 360) from E.I. Dupont were used to produce both the thin film and bulk samples. The physiochemical characteristics of both polymers are summarized in Table 1. The T_g of PS and the T_m of the EVA copolymer are well above room temperature, so that minimal mobility of the polymer occurs under ambient conditions. As reported by Koga et al.,[23] polymer mobility is only possible when exposed to the sc CO_2 density fluctuation regime. Hence, the morphology produced during exposure can be preserved, or "frozen" in shape, if the sc CO_2 pressure is rapidly released.

2.2. Thin Film Polymer Samples. The PS/EVA thin films were spun-cast onto hydrophobic Si (111) substrates. The Si wafers were cleaned using a modified Shirake technique where each wafer was first submerged in a boiling 1:1:1 H_2SO_4:H_2O_2:H_2O solution for 1 h and then oxide-etched in a 1:3 HF:H_2O for 5 min. All liquid chemicals used were of reagent grade.

A 50%−50% (w/w) solution of PS/EVA was prepared by dissolving the polymers in toluene. Toluene is an effective solvent for PS but requires heating in order to dissolve the EVA copolymer. Once the solution became clear, usually after 24 h, thin films of the blend were spun-cast onto Si wafers using a Headway Research model PWM32 Spinner. Then samples were annealed for 24 h in an oil-trapped Hotpack model 273600 vacuum-sealed oven at 175 °C to promote phase segregation. The samples were then exposed to sc CO_2 (anaerobic grade, 99.9998% pure) at 1100, 1900, 2500, and 3000 psig along a 36 °C isotherm 1 h. The topography and phase contact angles of the films were then studied with a DI-3100 scanning force microscope in the contact mode.

2.3. Bulk Polymer Samples. The macroscopic PS/EVA samples prepared in this study were molded to ASTM method D 638-91 shapes commonly referred to as "dog bones" in a Carver model C heat press after high-torque melt blending in a C.W. Brabender model 680D twin-screw extruder at 180 °C and 100 rpm for 20 min. The samples were exposed to sc CO_2 (anaerobic grade, 99.9998% pure) at 1100, 1900, 2500, and 3000 psig and 36 °C for 1 h.

Before and after sc CO_2 exposure, uniaxial tension testing was performed using a model 1000 Instron apparatus with a 1000 lb capacity model 45/8130-05 Sensotec load cell. Load and displacement data were collected electronically and normalized to sample dimensions, given as engineering tensile stress and strain.

Dynamic mechanical analysis (DMA) using a Mettler-Toledo model Tritec 2000 was used to determine dynamic storage moduli E' at near-ambient temperatures. Young's tensile moduli, given as the initial slope of the tensile stress−strain curve, were not reported, since too few data points were collected in this region to produce accurate slope values. Therefore, the DMA was considered a more indicative, reliable measure of sample moduli.

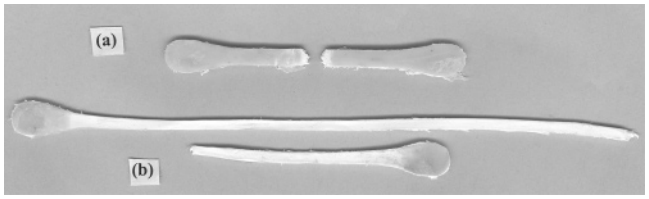

Figure 1. Optical images of EVA/PS blends after breakage in tensile test (a) unexposed sample and (b) after exposure to 1200 psig and 36 °C sc CO_2.

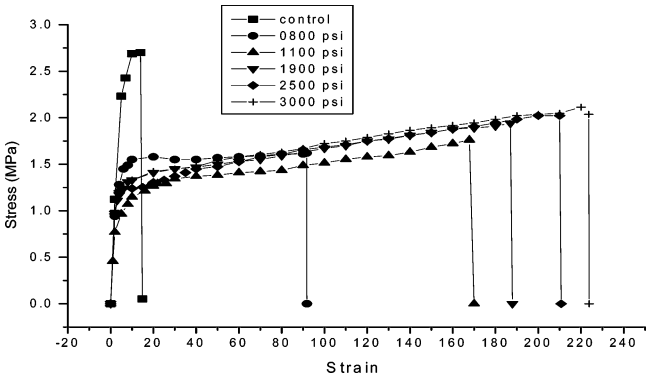

Figure 2. Stress vs strain data of bulk PS/EVA blends exposed to varying pressures of sc CO_2. The ductility was calculated from the area under the curve.

Differential scanning calorimetry (DSC) was performed using a Mettler-Toledo model DSC831E apparatus for measuring the glass transition T_g and melting point T_m of the materials at temperatures ranging from 0 to 150 °C. The temperature ramp rate was 10 °C/min for all samples studied. Liquid nitrogen was used to cool the samples to their initial temperatures. 280K g/mol M_w PS and ELVAX 360 were used.

In addition, the fractured edge of each bulk sample after tensile stress application was analyzed using a JEOL JSM5300 scanning electron microscope (SEM) from a viewpoint parallel to the direction of applied stress. This provides an image of the fractured surface porosity, spline dimensions, and domain size. Samples were then gold-sputter coated and scanned in the SEM.

3. Results and Discussion

3.1. Mechanical Properties. Figure 1 is an optical photograph of the "dog-bone" shape molds of the PS/EVA blend after tensile testing. From the figure we can see that exposure to sc CO_2 near $P = 1200$ psi and $T = 36$ °C produces a dramatic difference in both appearance and elongation of the materials. Prior to exposure, the sample elongated ∼130% under tensile loading. The plastic yield region is evident as the small white area surrounding the fracture. After exposure the sample was extended more than 600% before rupture. From the image it is clear that all of the material between the grips has undergone plastic deformation prior to fracture, which shows that the load-bearing regions were well-distributed throughout the material. The mechanical behavior is further quantified in Figure 2, where we show the entire engineering tensile stress vs engineering strain curves for samples exposed to sc CO_2 at different pressures. The parameters extracted from these curves are listed in columns 1−4 of Table 2. From the figure we find that the maximum load before yield, or the ultimate tensile stress (UTS), was reduced immediately after exposure to sc CO_2 at a pressure of

Table 2. Experimental Data for PS/EVA Bulk Blend Samples

sc CO_2 exposure pressure (psig) $T = 32$ °C	ductility[a] (MPa)	elongation ϵ (%)	tensile strength σ (MPa)	storage modulus E' (MPa)	DSC transitions (°C)	
					T_g	T_m
not exposed	94	134	2.70	115.0	102	73
800	434	239	1.62	42.8		
1100	754	557	1.76	30.1	30 and 102	73
1900	945	569	1.94	27.5		
2500	1075	625	2.02	28.5		
3000	1195	682	2.06	26.9		

[a] Calculated as the definite integral under the engineering stress−strain curve from zero to the strain of fracture.

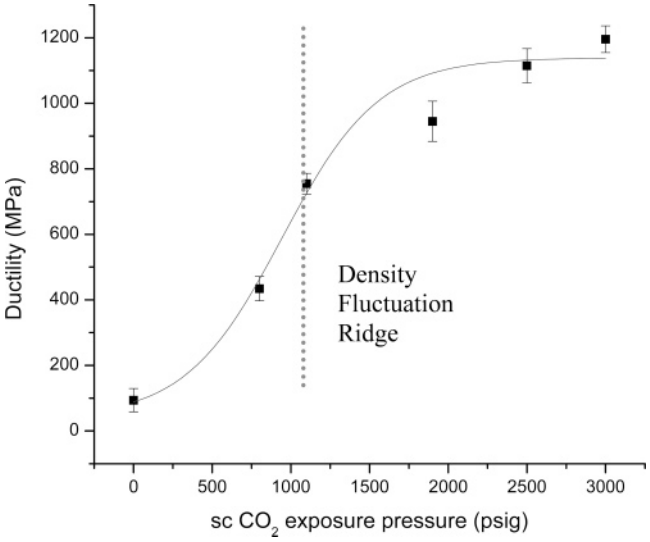

Figure 3. Ductility vs sc CO_2 pressure of bulk PS/EVA blends. The supercritical density fluctuation ridge is denoted by the dotted line on the graph.

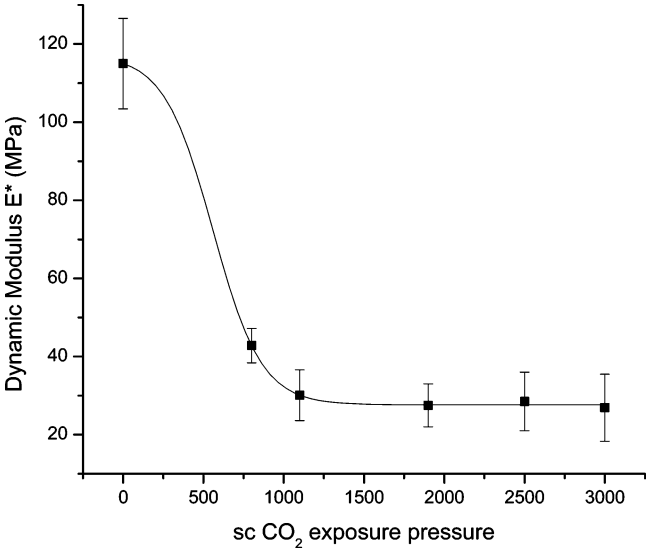

Figure 4. Modulus vs sc CO_2 exposure pressure of bulk PS/EVA blends.

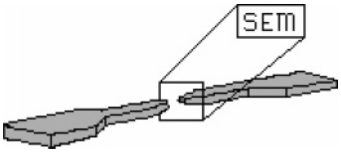

Figure 5. SEM vantage point. The bulk samples are broken under tensile stress and then imaged with SEM to observe the fracture morphology.

800 psi. Increasing the pressure further increased mostly the extension to break and the ductility of the samples. In Figure 3, we plot the ductility vs sc CO_2 exposure pressure at a fixed temperature of 36 °C. From the figure we find that an inflection point followed by a plateau occurs near $P = 1200$ psi. This pressure and temperature regime was shown by Nishikawa[19−21] to lie on the density fluctuation ridge for sc CO_2. This locus of points also coincides with the region where Koga et al.[22] report anomalous dilation of thin films of numerous polymers, including PS and EVA. Wissinger et al.[12] and Zhang et al.[13] also report anomalous swelling in bulk polymers, though to a lesser degree than in thin films. From the tensile data in Figure 2, one can see that Young's modulus, as determined by the slope of the linear elastic region on the engineering stress vs strain curves, cannot be very accurately measured due to scarcity of data in this region. However, more detailed measurements of the dynamic storage moduli were taken via DMA, as listed in column 5 of Table 2 and shown graphically in Figure 4. These data show a large decrease from 110 to 40 MPa immediately after exposure to $P = 800$ psi, followed by a plateau of 30 MPa after exposure to sc CO_2 at pressures up to 3000 psi. To understand the possible morphological reasons for this change in the mechanical properties, we studied the surfaces of the broken samples using SEM. The exact location of the scanned surfaces can be seen in Figure 5. SEM data are shown in Figure 6a−d. Prior to exposure the material is not very porous, and hence we postulate that it undergoes brittle fracture along the polymer−polymer phase boundaries. After exposure, however, we find increased porosity in the samples due to foaming in the sc CO_2. This finding is similar to the results reported by McCarthy et al.[2,5] and is due to the incompatibility of sc CO_2 with the polymer matrix, which causes it to phase segregate into spherical domains. When the pressure is released rapidly, the sc CO_2 returns to the gaseous state and is released faster than the relaxation time of the polymer matrix, leaving a "popcorn-like" impression in the bulk polymer. From Figure 6, we can estimate that the void regions after exposure have diameters of ∼5−15 μm, separated by dense polymer splines of ∼1−2 μm thickness at a density of 10^{10}−10^{14} cells/cm^3. Consequently, it appears that the materials are now undergoing ductile fracture due to the presence of the foam. Correlating these images with the mechanical properties, we can say that the lower dynamic modulii are also primarily due to the presence of the foam. The surfaces of each spline inside the pores are exposed to sc CO_2 during foaming, and hence the surface-to-volume ratio of the polymer is greatly increased.[4,5] On the other hand, another mechanism may play a role in the large increase in the ductility observed at higher pressures. This mechanism is not immediately apparent from the SEM images and requires more microscopic analysis.

When polymeric foams elongate, the tensile stress is concentrated in the splines of the foam. From Figure 3,

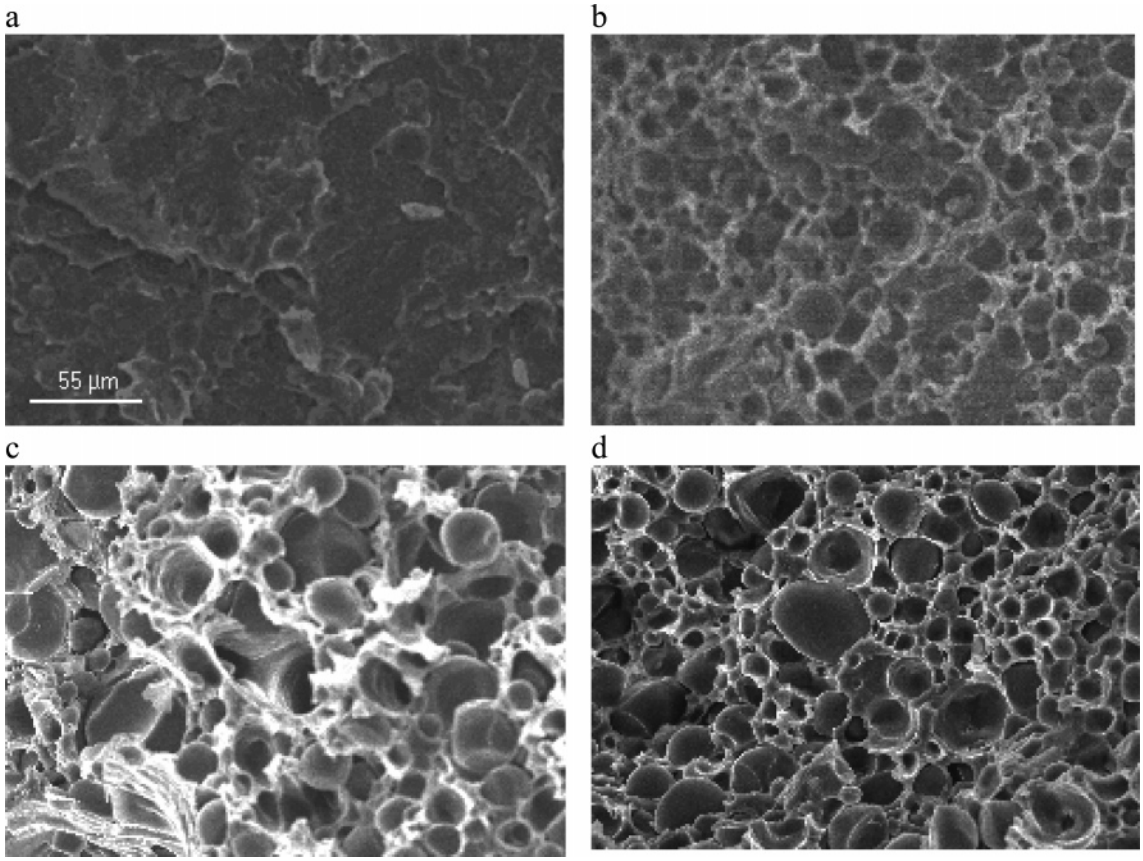

Figure 6. SEM images of bulk scale PS-EVA samples (a) before exposure to sc CO_2 and (b−d) after exposure to sc CO_2 on at 36 °C and pressures of 800, 1100, and 3000 psig, respectively. The 55 μm scale bar shown in image (a) applies to images (b−d) as well.

we see that the ductility increases sharply near P = 1100 psig and plateaus for higher pressures. From Figure 6b we know that the material is already partially foamed at P = 800 psig; hence, the inflection point in ductility must be due to another transformation within the splines. Since the original material is composed of an immiscible blend, the interfaces between the phase-separated polymer domains are narrow, and hence the adhesion is poor. This is reflected in the low ductility data and the brittle fracture surface SEM images observed in the unexposed samples. The large increase in ductility indicates that the internal adhesion becomes altered by the sc CO_2 system and not simply due to the foaming. There must therefore be a mechanism through which the tensile load-bearing splines are strengthened at pressures corresponding to the density fluctuation ridge. Koga et al.[26] have shown in situ miscibilization of polymer blends in this pressure−temperature region of sc CO_2 for thin film surfaces. They found that interfacial widths broadened by more than 300% when polymer bilayer films were exposed to sc CO_2 at pressures and temperatures along the density fluctuation ridge. This phenomenon was specific to thin films since the correlation length of the fluctuation domain was limited to a few polymer radii of gyration or ∼100 nm for entangled polymers. Hence, this phenomenon was not considered a significant factor in modifying the mechanical properties of solid bulk samples. However, when the polymer has a foam structure, as shown in Figure 6, the surface-to-volume ratio is greatly increased. Since the diameter of the splines can be on the order of a few hundred nanometers, the surface effects reported by Koga must become a very important factor. Any miscibilization between PS and EVA in this region would greatly increase the adhesion forces within the individual splines, making the bulk material far more ductile. This principle is illustrated in the cartoon drawing shown in Figure 6. The lighter regions on the splines represent where we claim the surface effect seen in thin films[24] also occurs within the cells of bulk polymer blend foams.

3.2. Thermal Analysis. The degree of miscibilization due to exposure to sc CO_2 along the fluctuation ridge was also studied using differential scanning calorimetry (DSC) of the pure polymers and the polymer blends. In this case we tested PS of both M_w = 45K and 280K g/mol, with identical results. The higher molecular weight samples were prepared just to ensure that the results were not affected by polydispersity of the lower molecular weight material. The data for the homopolymers and the blends of equal mass ratio are shown in Figure 8. From the first two traces in the figure we can see that the glass transition temperature of PS and the melting point of EVA are located near 102 and 73 °C, respectively, in agreement with literature values.[30] In the third trace, the PS/EVA blend prior to exposure, we observe transitions at 102 °C, corresponding to the T_g of PS, and at 70 °C, corresponding to the T_m of EVA. The last trace corresponds to the blend exposed to sc CO_2 on the density fluctuation ridge. Here we see a robust T_m peak at 74.6 °C, which clearly indicates that the crystallinity of the EVA component is not degraded by the exposure. We also observe a T_g peak at 102 °C, which corresponds to the PS homopolymer. A second T_g peak is now observed at T = 30.4 °C. This peak we believe is due to the miscibilized components of the

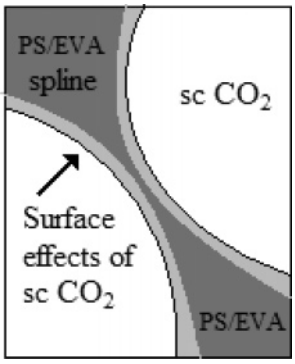

Figure 7. A magnified view of the splines between pores shown in Figure 5, which illustrates the increased surface to volume ratio due to the foaming process. The light gray region corresponds to the relative penetration depth of the sc CO_2 in the density fluctuation regime where Koga et al.[22] have demonstrated that miscibilization occurs.

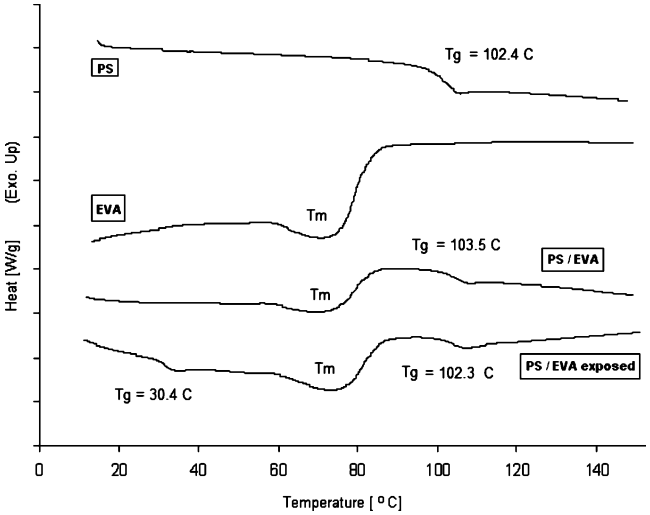

Figure 8. Differential scanning calorimetry traces obtained by 10 °C/min scans from PS, EVA, and PS/EVA unexposed and exposed blend samples. T_g and T_m denote the PS glass transitions and the EVA melting points.

blend near the surface of the splines. For a completely miscibilized blend of equal composition, the Flory−Fox relationship (eq 1) would predict a single T_g given by

$$\frac{1}{T_g} = \frac{w_1}{T_{g1}} + \frac{w_2}{T_{g2}} \tag{1}$$

where w_1, w_2, T_{g1}, and T_{g2} are the mole fractions and glass transitions of the pure components. Substituting the values from Table 1, this yields T_g = 19 °C. The deviations between the observed value at T_g = 30 °C and predicted values can easily be explained by the finite penetration depth of the sc CO_2 along the splines, as illustrated in Figure 7. The much larger difference between the first and second T_g peak is consistent with increased miscibilization in a significant fraction of the mass of the splines, which is large enough be responsible for the improved mechanical properties.

3.3. Interfacial Energies. Since there is very little X-ray or electron contrast between PS and EVA, it is difficult to measure the interfacial width of the phase segregated domains by either transmission electron microscopy or X-ray reflectivity of bilayer films. Consequently, we chose to measure the interfacial energies by directly measuring the Young's contact angle between coexisting phases at equilibrium. Thin films of equal weight fractions from the same polymers used to produce the bulk foams (PS, M_w = 45K g/mol and EVA, M_w = 100K g/mol) were spun-cast onto Si wafers and annealed in high vacuum at T = 170 °C for 24 h. Figure 9a is a scanning probe micrograph of the films after immediately annealing. From the figure we see that the films are phase segregated, which is expected for an immiscible system. The two phases are most apparent in the lateral force scan where the PS phase appears darker than the EVA phase. In this mode the amplitude of the deflections increases when the tip penetration is increased. Hence, the softer material provides a larger deflection of the tip and appears brighter while the harder polymer appears relatively darker. In the topography mode, we can measure the surface morphology of the films and obtain the equilibrium contact angle between the two phases. This technique has been successfully reported by Vitt and Shull,[28] Slep et al.,[29] and Yuan et al.[10] in various applications. The observed contact angle θ, obtained from averaging more than 12 droplets of various sizes, is 18 ± 1.8° before exposure to sc CO_2. In Figure 9b, we show the effect on the contact angle after exposure to sc CO_2 at P = 1200 psi and T = 36 °C, which are near the density fluctuation ridge studied by Koga et al.[24,25] From the scan we clearly see that the angle has decreased by more than 3 times to an average value of 6°, indicating that miscibilization had occurred through the exposure. In Figure 10 we plot the contact angle obtained by exposing other annealed films to sc CO_2 at T = 36 °C as a function pressure, where we see that a large decrease occurs as the ridge is approached. The values are tabulated in Table 3.

We can quantify the reduction in the interfacial tension between the polymers, as a function of pressure, using the classical Young's relation, eq 2.[30]

$$\gamma_{EVA} - \gamma_{PS} \cos\theta = \gamma_{PS/EVA} \tag{2}$$

We can substitute the known values for θ, γ_{PS}, and γ_{EVA} at 36 °C and solve for $\gamma_{PS/EVA}$ to obtain an initial interfacial tension of 3.49 dyn/cm prior to exposure. Jaeger et al.[31] have shown that the surface tension in vacuo of a polymer is unchanged by exposure to sc CO_2. Hence, we can substitute the reduced values of the contact angle into eq 1 to find the interfacial tension as a function of pressure. In Figure 10, we plot these data as a function of sc CO_2 exposure pressure, where we see that the interfacial tension is decreased by more than 30%, for samples exposed to pressures below and above the ridge. These findings are in close agreement with those of Li et al.[32] which reported increased miscibilization of bulk polymers in the same region of the sc CO_2 phase diagram. We can therefore infer that miscibility has been achieved in the films.

4. Conclusions

Significant enhancement of the mechanical properties in PS/EVA blends has been achieved via sc CO_2 exposure in the pressure/temperature domain where the amplitudes of the density fluctuations are maximal, also known as "the density fluctuation ridge" of the phase diagram. When blends were exposed to sc CO_2 at a constant temperature (36 °C), the ductility increased with pressure. The largest gradient occurred in the pressure domain corresponding to the ridge. Similarly, the ductility increased with the largest differential

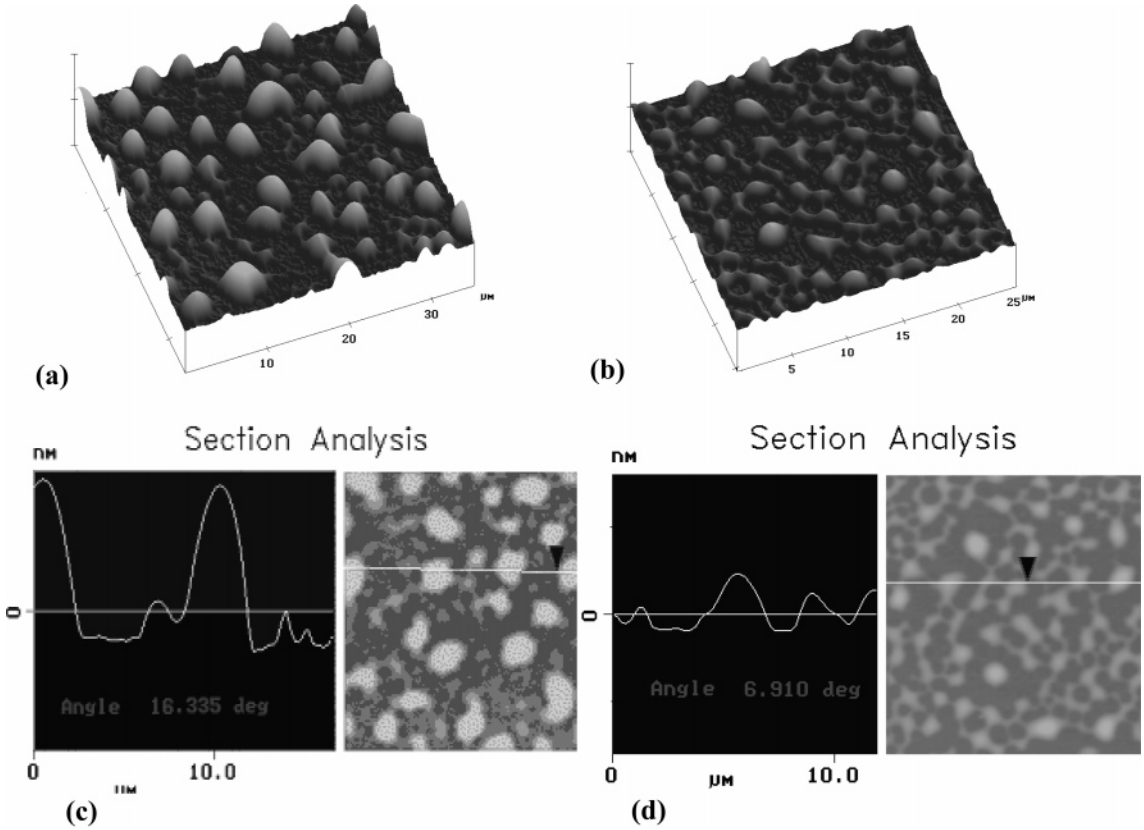

Figure 9. Thin (~100 nm) films of PS/EVA spun-cast onto a Si wafer and annealed for 24 h at 170 °C (a) before exposure to sc CO_2 and (b) after exposure to 1200 psig and 36 °C, on the density fluctuation ridge for sc CO_2. To the left of each figure is the cross-sectional trace used to calculate the contact angles.

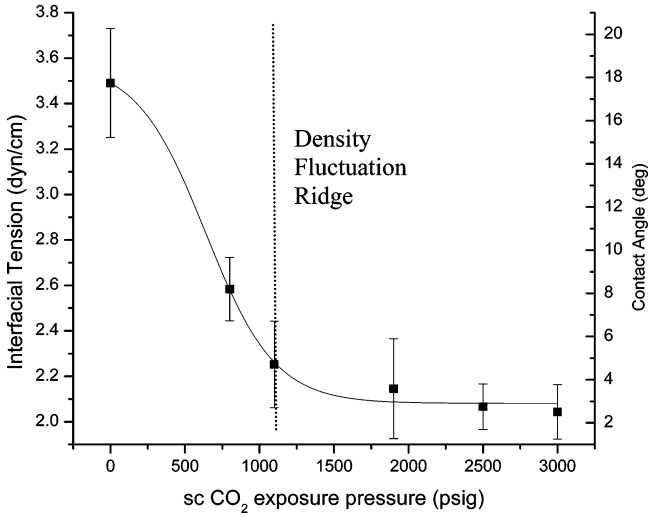

Figure 10. PS/EVA thin film interfacial tensions and equilibrium contact angles as a function of sc CO_2 exposure pressure. The vertical dotted line represents the ridge.

Table 3. Experimental Data for PS/EVA Thin Films

sc CO_2 exposure pressure (psig)	contact angle θ (deg)	interfacial tension γ (dyn/cm)
not exposed	17.8	3.5
800	11.1	2.6
1100	7.3	2.3
1900	5.6	2.2
2500	4.1	2.0
3000	3.0	2.0

around $P = 1100$ psi, which is also on the ridge. Before exposure, bulk samples of the blends elongated an average of 134% under uniaxial tension, whereas the average elongation was 682% after exposure. SEM micrographs of the exposed blends indicated that pores ~5−15 μm in diameter, separated by splines 1−2 μm wide, were formed due to all exposure pressures ≥800 psi, which is consistent with previously reported foaming phenomena in polymer systems.

Koga et al. have previously shown that sc CO_2 is universally miscible in polymer thin films and at polymer surfaces[35] along the density fluctuating ridge. We therefore proposed that enhancement of mechanical properties in PS/EVA was directly caused by an increased miscibilization of the immiscible polymers along the spline surfaces. When foaming occurs, the surface-to-volume ratio is increased, thereby increasing the regions where miscibilization can occur. Since tensile stresses in the material are concentrated in the splines, reinforcement of the mechanical properties in this specific area results in an overall enhancement of the tensile properties of the bulk material.

At least partial miscibilization in the bulk material was confirmed thermally by observing a shift in the polystyrene T_g from near 104 °C in the initial blend to 31 °C after sc CO_2 exposure, using DSC. Using the classical Flory−Fox relationship, we determined that miscibilization must be occurring in a significant portion of the bulk material. Also, exposing spun-cast thin films of PS/EVA, phase segregated by annealing above the glass transition, confirms miscibilization at these surfaces due to sc CO_2. AFM analyses indicated that the contact angle between the two phases decreased from 18° to 3°. This corresponded to a decrease in the interfacial tension from 3.5 dyn/cm before to 2.0 dyn/cm after exposure to sc CO_2 in the density fluctuation regime. More direct evidence of compatibilization can

of course be obtained from transmission electron microscopy of microtomed cross sections of the splines as well as small-angle neutrons scattering (SANS) determination of the domain size and interfacial broadening. Because of the low T_g values of the EVA, the mechanical rigidity of the splines was too low to enable accurate cross sectioning to be performed, though SANS experiments are currently in progress. These studies will be published elsewhere. We should note that similar experiments were conducted for the glassy polymer system, deuterated polystyrene, and poly(methyl methacrylate) blends where initial results show large segregated domains in the unexposed samples and nearly uniform regions in the splines of the exposed samples.[36]

Acknowledgment. This work was supported in part by the National Science Foundation MRSEC, RET programs, and the Siemen's Foundation.

References and Notes

(1) *Supercritical Fluid Extraction: Principles and Practice*; McHugh, M. A., Krukonis, V., Eds.; Butterworth-Heinemann: Woburn, MA, 1994.
(2) Stafford, R.; Russell, T. P.; McCarthy, T. J. *Macromolecules* **1999**, *32*, 7610−7616.
(3) Sun, H.; Sur, G. S.; Mark, J. E. *Eur. Polym. J.* **2002**, *38*, 2373−2381.
(4) Sun, H.; Mark, J. E. *J. Appl. Polym. Sci.* **2002**, *86*, 1692−1701.
(5) Arora, K. A.; Lesser, A. J.; McCarthy, T. J. *Macromolecules* **1999**, *32*, 2562−2568.
(6) Chang, S. H.; Park, S. C.; Shim, J. J. *J. Supercrit. Fluids* **1998**, *13*, 113.
(7) Elkovitch, M. D.; Lee, L. J.; Tomasko, D. L. *Polym. Eng. Sci.* **2000**, *40*, 1850.
(8) Elkovitch, M. D.; Lee, L. J.; Tomasko, D. L. *Polym. Eng. Sci.* **2001**, *41*, 2108−2118.
(9) Walker, T.; Raghavan, R. J.; Smith, S.; Wignall, G.; Melnichenko, Y.; Khan, S.; Spontak, R. *J. Phys. Chem.* **1999**, *103*, 5472; *Macromol. Chem. Phys.* **2003**, *204*, 2064−2077.
(10) Yuan, C. G.; Meng, O. Y.; Koberstein, J. T. *Macromolecules* **1999**, *32*, 2329−2333.
(11) Tomasko, D. L.; Han, X. M.; Liu, D. G. *Curr. Opin. Solid State Mater. Sci.* **2003**, *7*, 407−412.
(12) Cansell, F.; Aymonier, C.; Loppinet-Serani, A. *Curr. Opin. Solid State Mater. Sci.* **2003**, *7*, 331−340.
(13) Kikic, I.; Vecchione, F. *Curr. Opin. Solid State Mater. Sci.* **2003**, *7*, 399−405.
(14) Alessi, P.; Cortesi, A.; Kikic, I.; Vecchione, F. *J. Appl. Polym. Sci.* **2003**, *88*, 2189−2193.
(15) McHugh, M. A.; Park, I. H.; Reisinger, J. J.; Ren, Y.; Lodge, T. P.; Hillmyer, M. A. *Macromolecules* **2002**, *35*, 4653−4657.
(16) Royer, J. R.; Gay, Y. J.; Adam, M.; DeSimone, J. M.; Khan, S. A. *Polymer* **2002**, *43*, 2375−2383.
(17) Reverchon, E.; Volpe, M. C.; Caputo, G. *Curr. Opin. Solid State Mater. Sci.* **2003**, *7*, 391−397.
(18) Meli, L.; Pham, J. Q.; Johnston, K. P.; Green, P. F. *Phys. Rev. E.* **2004**, *69*, Art. No. 051601.
(19) Pham, J. Q.; Johnston, K. P.; Green, P. F. *J. Phys. Chem. B* **2004**, *108*, 3457−3461.
(20) Goel, S. K.; Beckman, E. J. *Polymer* **1993**, *34*, 1410.
(21) Nishikawa, K.; Tanka, I.; Amemiya, Y. *J. Phys. Chem.* **1996**, *100*, 418−421.
(22) Nishikawa, K.; Ochiai, H.; Saitow, K. *J. Chem. Phys.* **2003**, *286*, 421−430.
(23) Nishikawa, K.; Kusano, K.; Arai, A. A. *J. Chem. Phys.* **2003**, *118*, 1341−1346.
(24) Koga, T.; Seo, Y. S.; Hu, X.; Shin, K.; Zhang, Y.; Rafailovich, M. H.; Sokolov, J. C.; Chu, B.; Satija, S. K. *Europhys. Lett.* **2002**, *60*, 559−565.
(25) Koga, T.; Seo, Y.; Shin, K.; Zhang, Y.; Rafailovich, M. H.; Sokolov, J. C.; Chu, B.; Satija, S. K. *Macromolecules* **2003**, *36*, 5236−5243.
(26) Koga, T.; Seo, Y.; Shin, K.; Kusano, K.; Nishikawa, K.; Rafailovich, M.; Sokolov, J.; Chu, B.; Peiffer, D.; Occhiogrosso, R.; Satijs, S. *Phys. Rev. Lett.* **2002**, *89*, 125506-1.
(27) Kung, E.; Lesser, A. J.; McCarthy, T. J. *Macromolecules* **1998**, *31*, 4160−4169.
(28) Vitt, E.; Shull, K. R. *Macromolecules* **1995**, *28*, 6349−6353.
(29) Slep, D.; Asselta, J.; Rafailovich, M.; Sokolov, J.; Winsett, D.; Smith, A.; Ade, H.; Anders, S. *Langmuir* **2000**, *16*, 2369−2375.
(30) *Polymer Handbook*, 4th ed.; Bradrup, J., Immergut, E. H., Eds.; John Wiley & Sons: New York, 1999 and http://www.dupont.com/industrial-polymers/elvax/pdfs/vax360.pdf.
(31) Jaeger, P. T.; Eggers, R.; Baumgartl, H. *J. Supercrit. Fluids* **2002**, *24*, 203.
(32) Li, H. B.; Lee, L. J.; Tomasko, D. L. *Ind. Eng. Chem. Res.* **2004**, *43*, 509−514.
(33) Wissinger, R. G.; Paulaitis, M. E. *J. Polym. Sci., Phys. Ed.* **1987**, *25*, 2497.
(34) Zhang, Y.; Gangwani, K. K.; Lemert, R. M. *J. Supercrit. Fluids* **1997**, *11*, 115.
(35) Koga, T.; Seo, Y. S.; Hu, X.; Shin, K.; Zhang, Y.; Rafailovich, M. H.; Sokolov, J. C.; Chu, B.; Satija, S. K. *Europhys. Lett.* **2002**, *60*, 559−565.
(36) Fourman, M. S.; Palermo, E.; Occhiogrosso, R.; Rafailovich, M.; Sokolov, J.; Si, M.; Koga, T.; Jerome, J. Proceedings of the MRS Fall Meeting, Boston, MA, Nov 2004 and to be published.

MA051335+